CDF/PUB/EXOTICS/PUBLIC/10603

Search for High-Mass Resonances Decaying into ZZ in $p\bar{p}$ Collisions at $\sqrt{s} = 1.96\,\mathrm{TeV}$

(Dated: July 17, 2011, version 3.00)

We search for high-mass resonances decaying into Z boson pairs using data corresponding to $6\,\mathrm{fb}^{-1}$ collected by the CDF experiment in $p\bar{p}$ collisions at $\sqrt{s} = 1.96\,\mathrm{TeV}$. Eight $p\bar{p} \to ZZ \to \ell^+\ell^-\ell^+\ell^-$ events are observed, of which four have invariant masses M_{ZZ} consistent with $327\ \mathrm{GeV}/c^2$, and also have unexpectedly high values of $p_T(ZZ)$. However, analysis of the $ZZ \to \ell^+\ell^-\nu\nu$ and $ZZ \to \ell^+\ell^- jj$ final states does not confirm a heavy resonance decaying into a pair of Z bosons. 95% CL upper limits are set on the production cross section times branching ratio $\sigma(p\bar{p} \to X \to ZZ)$ at 0.26 pb and 0.28 pb for two signal models.

PACS numbers:

I. INTRODUCTION

We report the results of a search for high-mass resonances decaying to ZZ in $p\bar{p}$ collisions at $\sqrt{s} = 1.96\,\mathrm{TeV}$ at the Tevatron. New physics could affect ZZ production in different ways. In models containing large extra dimensions the ZZ production cross section is increased through loop corrections [1]. Resonances appearing at high mass such as a Higgs boson or Randall-Sundrum (RS) graviton [2] could decay manifestly to two Z bosons. The decay of the standard model Higgs boson to ZZ is expected to be beyond the sensitivity of the Tevatron experiments [3]. The original RS model predicts Kaluza Klein excitations G^* of the graviton that decay predominantly to a pair of charged leptons or a pair of photons, and experimental searches for such high-mass resonance decays have excluded RS graviton states up to a mass of around $1\,\mathrm{TeV}/c^2$ at 95% confidence level for a natural choice of coupling parameter [4], both at the Tevatron and at the LHC [5]. However in RS models that have standard model fields propagating in the bulk, the G^* couplings to light fermions and photons may be heavily suppressed so that the dominant decay modes are to $t\bar{t}$, Higgs pairs, or pairs of heavy bosons [6]. Furthermore, in some models the decay to heavy bosons is dominant [7]. Suppression of the couplings to light fermions also results in gluon fusion becoming the primary production process.

The CDF experiment has previously looked for resonances decaying to Z pairs and excluded an RS graviton up to a mass of around $0.5\,\mathrm{TeV}/c^2$ at 95% confidence level [8]. The search described in this paper gives improved sensitivity over the previous analysis through modified event selection, the inclusion of extra final states, and the addition of more data. Three final states are analysed, corresponding to the different Z boson decay modes $ZZ \to \ell^+\ell^-\ell^+\ell^-$, $ZZ \to \ell^+\ell^-\nu\nu$, and $ZZ \to \ell^+\ell^- jj$, where ℓ is an electron or muon and j is a hadronic jet. These three channels have different signal-to-background ratios and allow an overconstrained search. The $\ell\ell\ell\ell$ final state has the smallest background; however, depending on the resonance mass, the best single-channel sensitivity is provided by either the $ZZ \to \ell^+\ell^- jj$ or $ZZ \to \ell^+\ell^-\nu\nu$ channels. In this paper we report unexpected events in the $ZZ \to \ell^+\ell^-\ell^+\ell^-$ channel, and seek confirmation from the other channels.

The paper is organised as follows: in Section II we introduce the CDF detector and trigger system; in Section III we describe the reconstruction and identification procedures; then in Sections IV–VI we report the search results from each of the channels $ZZ \to \ell^+\ell^-\ell^+\ell^-$, $ZZ \to \ell^+\ell^-\nu\nu$ and $ZZ \to \ell^+\ell^- jj$. Section VII gives limits resulting from all three channels and their combination.

II. DETECTOR

The CDF II detector is a general purpose particle detector, described in detail elsewhere [9]. The results reported in this paper use information from several detector subsystems for charged lepton and jet reconstruction and identification.

Tracks are reconstructed in the silicon system [10] and in the central tracker [11], which is a drift chamber that consists of 96 layers of sense wires grouped into eight 'superlayers'. Superlayers alternate between an axial configuration, with sense wires parallel to the colliding beams, and a small-angle stereo configuration. For high momentum tracks the resolution is $\sigma_{p_T}/p_T^2 \simeq 1.7 \times 10^{-3}(\mathrm{GeV}/c)^{-1}$, where $p_T = p\sin\theta$, p being the track momentum and θ the polar angle with respect to the proton direction.

The calorimeter is segmented radially into electromagnetic and hadronic compartments [12, 13]. The central calorimeter is split at the center into two separate barrels and covers $|\eta| < 1.1$ (where $\eta = -\ln\tan\frac{\theta}{2}$). Each barrel consists of 24 azimuthal wedges segmented in projective towers of 0.1 in η. The forward calorimeter segmentation increases from 0.1 in η and 7.5° in ϕ at $\eta = 1.1$, to 0.5 in η and 15° in ϕ at $\eta = 3.6$. Electron energy resolutions are $13.5\%/\sqrt{E_T} \oplus 2\%$ in the central calorimeter and $16\%/\sqrt{E_T} \oplus 1\%$ in the forward calorimeters, where $E_T = E\sin\theta$. The electromagnetic calorimeters incorporate shower maximum detectors that are used to measure shower profiles with spatial resolution of around 2 mm.

Dedicated muon detectors [14] are mounted around the calorimeters, providing coverage for $|\eta| \lesssim 1.5$. Luminos-

ity is measured by a hodoscopic system of Cherenkov counters [15].

CDF has a three-level online trigger system. The data used in this measurement were collected using inclusive high-p_T electron and muon triggers, and a two-electron trigger. The single lepton triggers select events that have electron or muon candidates with $p_T \geq 18\,\mathrm{GeV}/c$ and $|\eta| \lesssim 1.0$ [16], and the two-electron trigger uses only calorimeter information and allows electron candidates above the same p_T threshold anywhere in the detector. The data correspond to an integrated luminosity of $6\,\mathrm{fb}^{-1}$ collected between February 2002 and February 2010.

III. RECONSTRUCTION AND IDENTIFICATION

In this section we discuss lepton reconstruction and identification, and jet and missing transverse energy reconstruction.

A. Leptons

Decays of a heavy resonance to ZZ, where at least one of the Z bosons decays leptonically, result in a wide lepton energy spectrum. Any inefficiency in lepton reconstruction and identification is raised to the fourth power in the $ZZ \to \ell^+\ell^-\ell^+\ell^-$ channel. Thus, keeping efficiency high while maintaining background rejection is equally important for $p_T \sim 20\,\mathrm{GeV}/c$ and for $p_T > 100\,\mathrm{GeV}/c$. To this end, this analysis incorporates several refinements in the offline reconstruction and identification of electron and muon candidates. Studies were performed on inclusive $Z \to \ell^+\ell^-$ events and on events containing one lepton plus two additional tracks, and this latter dataset was fully reprocessed for the $ZZ \to \ell^+\ell^-\ell^+\ell^-$ analysis.

First we describe the elements of the lepton selection that are standard to CDF. Electron candidates consist of a calorimeter cluster and a well-reconstructed matched track. Candidates are required to be fiducial to the shower maximum detectors and have a shower that is mostly contained in the electromagnetic compartment of the calorimeter, with a shower shape that is consistent with expectation. For candidates reconstructed in the central part of the detector ($|\eta| < 1.1$), the matched track must have p_T>10 GeV/c, pass through all layers of the central tracker, and have χ^2/d.o.f. < 3. Candidates reconstructed in the forward part of the detector, $1.13 < |\eta| < 2.8$, must either have hits in the central tracker, or ≥ 5 silicon hits.

A muon candidate is reconstructed from a track in the central tracker and track segments in the muon systems. Muon track trajectories must be such that at least 30 central tracker hits would be expected, and at least 60% of those must be found. Tracks pointing forward that have fewer than three central tracker segments must also have at least five $r-\phi$ hits in the silicon tracking system. Muon energy deposition must be consistent with that of a minimally-ionising particle: $E_{EM} < 2\,\mathrm{GeV}$ and $E_{HAD} < 6\,\mathrm{GeV}$. We also consider minimally-ionising muon candidates that do not have track segments in the muon systems.

Lepton candidates analysed in this paper are required to have $E_T > 15\,\mathrm{GeV}$ ($p_T > 15\,\mathrm{GeV}/c$ for muons). In addition, one of the lepton candidates in each event is also required to have $E_T > 20\,\mathrm{GeV}$ ($p_T > 20\,\mathrm{GeV}/c$ for muons) and to pass more restrictive quality requirements. These extra requirements are that the lepton track must have at least three segments reconstructed in the axial superlayers and three in the stereo superlayers; and the track of a muon candidate must also be well-matched to a track segment reconstructed in the muon system.

The first refinement in lepton selection is in the isolation requirement made on all lepton candidates. The 'isolation energy' is the amount of energy reconstructed in a cone of ΔR<0.4 around a lepton candidate. In computing the isolation energy we refine the treatment of energy leakage across calorimeter cell boundaries. In the central calorimeter, electron clusters include energy depositions from only a single wedge in ϕ. As each calorimeter tower is read out from different ϕ sides by two photomultiplier tubes, the relative heights of the pulses locate the energy deposition in ϕ. Knowing the location of the center of the energy depositions in towers neighbouring the electron cluster allows us to estimate the leakage and correct the isolation energy variable event-by-event, rather than by applying an average correction. The correction method is validated by examining the isolation energy as a function of shower position in the calorimeter cell, which is found to be much flatter than using the standard average correction, as shown in Fig. 1.a. Muons are not expected to result in energy leakage and their isolation energy is also shown in Fig. 1.a as validation of the method. The average isolation energy should depend on the instantaneous luminosity but not on the lepton E_T, as confirmed by Fig. 1.b. All electron and muon candidates are therefore required to be isolated in the calorimeter by limiting the isolation energy to be below 4 GeV, rather than cutting on isolation energy divided by lepton E_T, as is often done in CDF analyses. By doing so we increase the acceptance for $ZZ \to \ell^+\ell^-\ell^+\ell^-$ events by 4%.

For the $ZZ \to \ell^+\ell^-\ell^+\ell^-$ analysis, events have been reconstructed with an updated version of the CDF tracking code that gives improved pattern recognition at high luminosities. The updated version includes an extra pass to associate hits in the central tracker with silicon-only tracks from electron candidates in the forward region of the detector. Adding extra hits on to the tracks improves the robustness of forward electron charge identification.

Use of an improved reconstruction algorithm in the central shower maximum detector (CES) gives separation between showers generated by electron tracks and showers produced by bremsstrahlung photons. Matching tracks to the showers they initiate in both coordinate and energy improves hadron rejection and allows the inclu-

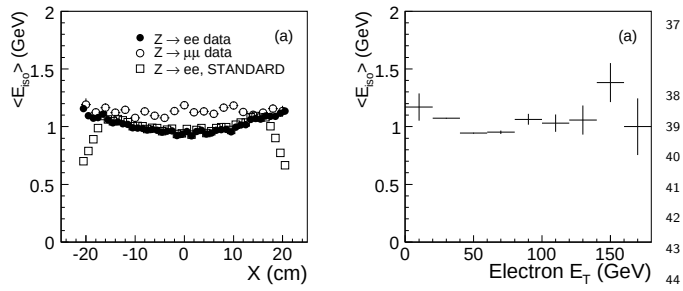

FIG. 1: a) Corrected isolation energy across the calorimeter wedge coordinate X in $Z \to e^+e^-$ (new correction: solid circles; standard correction: open squares) and $Z \to \mu^+\mu^-$ (new correction: open circles) events.
b) average calorimeter isolation energy as a function of electron E_T in $Z \to e^+e^-$ events.

sion of electron candidates that lose a significant amount of energy through bremsstrahlung. The improved background rejection allows the relaxation of other standard electron identification requirements and, overall, the selection efficiency is increased by around 9% per electron.

Electrons reconstructed in the edge ϕ-rings of the calorimeter on either side of the gap between the central and forward detectors are generally excluded from CDF analysis. They are included here, after verification that they have energy resolution comparable with electrons reconstructed in the bulk of the detectors, and are well-modeled in the simulation. This increases electron acceptance by around 10% per electron.

The combined effect of the refinements described above is to increase lepton acceptance without increasing fake lepton backgrounds, as measured by jet-to-lepton fake rates in inclusive jet datasets. The lepton selection used for analysis is validated by measuring inclusive $Z \to \ell^+\ell^-$ cross-sections and separating events by calorimeter region and muon system. We verify that for each subset of events the measurement is stable in time, and combining all channels we measure $\sigma(p\bar{p} \to Z) \times Br(Z \to \ell^+\ell^-) = (247 \pm 6(\text{stat.+syst.}) \pm 15(\text{lumi.}))$ pb, consistent with CDF's measurement [16].

B. Jets and $\not\!\!E_T$

Jets are reconstructed as clustered energy depositions in the calorimeter using a fixed cone algorithm with cone size $\Delta R = 0.4$ [17]. Jet energies are corrected for relative detector response and for multiple interactions, and we consider jets having $E_T > 20\,\text{GeV}$.

The missing transverse energy ($\not\!\!E_T$) is defined as the sum over calorimeter tower energies $\not\!\!E_T = -|\sum_i E_T^i \mathbf{n_i}|$, where $\mathbf{n_i}$ is the unit vector in the transverse plane that points to calorimeter tower i. The $\not\!\!E_T$ is adjusted to account for the energy corrections made to reconstructed jets, and for muons identified in the event.

IV. $ZZ \to \ell^+\ell^-\ell^+\ell^-$ CHANNEL

The first search channel is $ZZ \to \ell^+\ell^-\ell^+\ell^-$. We select events with four candidate charged leptons, which may be electrons or muons. At least two of the four must have $E_T > 20\,\text{GeV}$ ($p_T > 20\,\text{GeV}/c$) and pass the more restrictive lepton selection; and in order to have the trigger efficiency well-defined, at least one must satisfy the trigger requirements.

Leptons of the same flavour are paired to form Z candidates, seeded by a lepton that passes the tighter selection. In the case of four-electron or four-muon candidates, the pairings that minimize the χ^2 of the ZZ hypothesis are chosen:

$$\chi^2 \;=\; (M_{12} - M_Z)^2/\sigma_M^2 + (M_{34} - M_Z)^2/\sigma_M^2,$$

where M_{12} and M_{34} are the masses of the lepton pairs, $\sigma_M = 3$ GeV/c^2 approximates experimental resolution in $M_{\ell\ell}$ for both electron and muon decays, and M_Z is the mass of the Z boson.

We find ten events that pass the four-lepton selection. In all of these events the number of leptons of the same flavour is even. The best pairings of the ten candidate events are all oppositely-charged. To minimize the effect of Z/γ^* interference, both Z boson candidates are required to be within 15 GeV/c^2 of the Z pole, $76 < m_{\ell\ell} < 106$ GeV/c^2. Eight event candidates remain: two events have four reconstructed electrons ($eeee$), three have two electrons and two muons ($ee\mu\mu$), and the remaining three have four reconstructed muons ($\mu\mu\mu\mu$). The two events that fail the Z mass requirement both have one Z candidate with invariant mass below 60 GeV/c^2.

We use the selected events to measure the $p\bar{p} \to ZZ$ production cross section, assuming a standard model source.

On- and off-shell ZZ production followed by Z boson decays to charged leptons is the only standard model process that results in a final state with four high-p_T leptons produced in the primary interaction. The background in this channel thus comes only from misidentification. The main contributions are: $p\bar{p} \to WZ$ + jet with a jet misidentified as a lepton; $p\bar{p} \to Z + 2$ jets with both jets misidentified as leptons; and $p\bar{p} \to Z + \gamma$ + jet with both the photon and the jet misidentified as electrons. The contribution from $t\bar{t}$ production is an order of magnitude smaller than that of WZ production. As a result of the $M_{\ell\ell}$>76 GeV/c^2 requirement, the contribution of $Z \to \tau\tau$ decays is negligible.

The PYTHIA event generator [18] and the full CDF detector simulation [19] are used to simulate kinematics of these processes. Jet-to-lepton misidentification rates are measured in inclusive jet data and found to be of the order of 10^{-4}–10^{-3} per jet in the E_T range of 15–100 GeV. These misidentification rates are used to weight the simulated events of the background processes, resulting in a total background yield estimated to be less than 0.01

event.

The acceptance for standard model $p\bar{p} \rightarrow ZZ \rightarrow \ell^+\ell^-\ell^+\ell^-$ is determined using the leading order PYTHIA generator and found to be 0.13. In order to estimate the uncertainty arising from higher-order generator effects the MC@NLO generator is used [20], interfaced to HERWIG [21] to provide parton showering. The corresponding uncertainty on the acceptance is estimated to be 2.7%.

We also consider systematic effects due to the lepton identification and trigger efficiency. Lepton identification efficiencies are measured in the data using $Z \rightarrow \ell^+\ell^-$ events with uncertainties at the level of 1%. We also account for a small drop in lepton identification efficiency with time and assign a 2% uncertainty per lepton for residual run-dependent effects. We assume no correlation between the uncertainties on electron and muon reconstruction, and full correlation between the uncertainties for leptons of the same flavour. The trigger efficiency per four-lepton event is close to unit, with a systematic uncertainty of less than 0.5%. The total uncertainty on the four-lepton acceptance coming from lepton reconstruction and identification and from trigger efficiencies is thus 10%.

The branching fraction for two Z bosons to decay to electrons or muons is 4.52×10^{-3}. The scale factor to take into account differences in triggering, reconstruction and identification efficiencies between data and simulation is 0.8 ± 0.08, and the integrated luminosity is $5.91 \pm 0.35\,\mathrm{fb}^{-1}$, so eight observed events result in a cross-section:

$$\sigma(p\bar{p} \rightarrow ZZ) \;=\; (2.8\,^{+1.2}_{-0.9}\;(\mathrm{stat.}) \;\pm\; 0.3\;(\mathrm{syst.}))\,\mathrm{pb}$$

where the statistical uncertainty is the 68% confidence interval given by the method of Feldman and Cousins [22]. The central value is twice that of the theoretical prediction $(1.4 \pm 0.1)\,\mathrm{pb}$ [23]. However, the statistical uncertainty is large and the 90% confidence level band, $1.4\,\mathrm{pb} < \sigma(p\bar{p} \rightarrow ZZ) < 4.9\,\mathrm{pb}$, includes the theoretical prediction.

We find that the cross section is larger than expected due to an excess of events at high invariant mass (M_{ZZ}). The invariant masses of four events are clustered around $325\,\mathrm{GeV}/c^2$, as shown in Fig. 2. The average mass is $327\,\mathrm{GeV}/c^2$, and all four candidates, one $eeee$, one $ee\mu\mu$, and two $\mu\mu\mu\mu$, have values of M_{ZZ} within 7 GeV of the mean. In the four lepton channel the detector resolution $\sigma(M_{ZZ}) \sim 5 - 6\,\mathrm{GeV}/c^2$ so within detector resolution the invariant masses of all four candidates are consistent with being measurements of the same mass.

To study the possibility that these events are due to a decay of a heavy resonance, we split the eight candidate events into low- and high-mass samples and compare the properties of the events in the two samples. The high-mass region is defined by an a posteriori choice $M_{ZZ} > 300\,\mathrm{GeV}/c^2$, which is $\sim 5\sigma(M_{ZZ})$ below the observed clustering of events; less than 25% of the expected

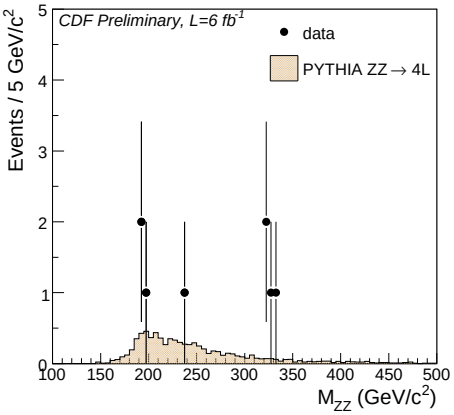

FIG. 2: M_{ZZ} for eight $ZZ \rightarrow \ell^+\ell^-\ell^+\ell^-$ candidates (PYTHIA normalised to standard model prediction of 5.8 events).

standard model M_{ZZ} distribution lies above this cutoff.

The masses of the Z candidates for all events are shown in Fig. 3, which demonstrates that the energy resolution is the same for the high-mass and low-mass events. Lepton identification variables are consistent with expec-

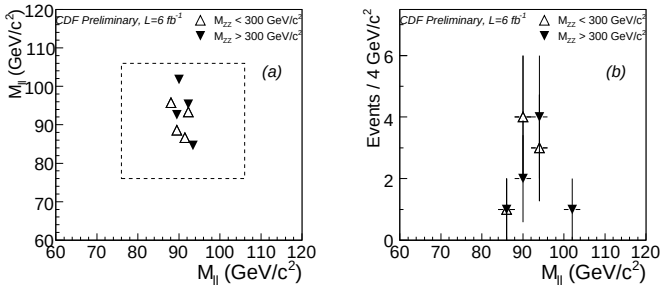

FIG. 3: Invariant masses of dilepton pairs in eight ZZ candidate events: (a) $M_{\ell\ell}(1)$ versus $M_{\ell\ell}(2)$, with selected mass region outlined; and (b) $M_{\ell\ell}$ for all Z boson candidates.

tation for all the observed events. Most kinematic distributions for the $ZZ \rightarrow \ell^+\ell^-\ell^+\ell^-$ candidates are in agreement with standard model expectation; as one example, the p_T distributions of the 16 Z bosons are shown in Fig. 4.

However for the high-mass events, the p_T distribution of the four lepton system is rather different from the standard model expectation, as shown in Fig. 5. The ZZ system in the high-mass events is seen to be boosted and, as shown in Fig. 6, is recoiling against one or more jets. None of the four low-mass events has a reconstructed jet above 20 GeV.

To assess the possibility that the high-mass events come from a non-standard model source, we exploit two models. The first model is RS graviton production through gluon-gluon fusion (the 's-channel signal model'). In order to investigate effects of the production mechanism and in the absence of a particular model that

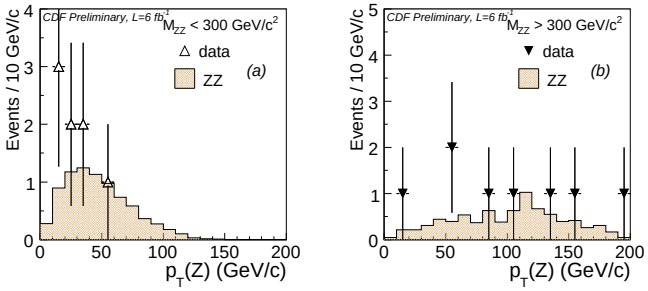

FIG. 4: $p_T(Z)$ for Z boson candidates in (a) low-mass four-lepton candidate events and (b) high-mass events (PYTHIA prediction normalised to four events in each plot).

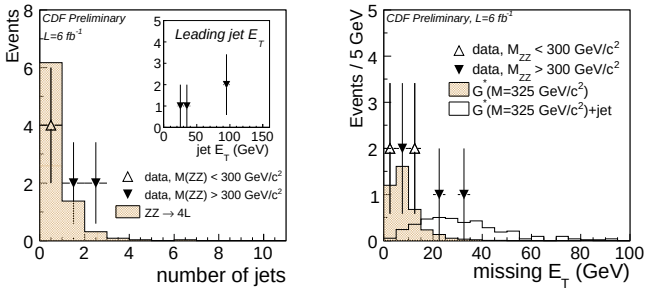

FIG. 6: (a) Number of jets and (inset) E_T of leading jet; and (b) $\not\!\!E_T$ for four-lepton candidate events. $\not\!\!E_T$ distribution for G*+jet process is normalized to 4 events.

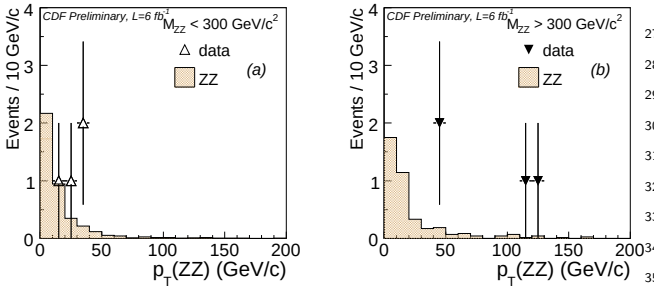

FIG. 5: $p_T(ZZ)$ for (a) low-mass four-lepton candidate events and (b) high-mass events (PYTHIA prediction normalised to four events in each plot).

would predict the production of a boosted ZZ resonance, we take as an alternative signal model the production of G^* with $M_{G^*} = 325\,\mathrm{GeV}/c^2$ recoiling against a parton of $E_T \geq 100\,\mathrm{GeV}$(referred to as the 'boosted signal model'). In both cases the HERWIG event generator is used with the full CDF detector simulation.

We check whether there is any indication of misreconstruction in these events. In $ZZ \to \ell^+\ell^-\ell^+\ell^-$ events, such an indication could come from large $\not\!\!E_T$. We study the $\not\!\!E_T$ distributions for the ZZ candidates, shown in Fig. 6. Comparison with the Monte Carlo predictions demonstrates that the measured $\not\!\!E_T$ is consistent with what is expected from resolution effects, where in the high-mass region, the resolution in $\not\!\!E_T$ is broadened by the presence of an extra jet.

Overall, we conclude that the observed events are well-measured and that, within the detector resolution, the kinematic parameters of the Z candidates are reconstructed correctly. The event properties are given in Table I.

In the absence of a physics model that would predict the observed properties of the high-mass ZZ candidate events, we quantify consistency between the data and the standard model by computing probabilities for the distributions observed in the data to be due to statistical fluctuations of the standard model expectations. First considering the clustering of events in M_{ZZ}: for a mean of 5.8 events expected from standard model production, the probability of observing four or more ZZ events that have $M_{ZZ} > 300\,\mathrm{GeV}/c^2$, with M_{ZZ} values of at least four of them within a $20\,\mathrm{GeV}/c^2$ window (which corresponds to approximately $\pm 2\sigma$ in resolution) is in the range $(2.3 - 5.2) \times 10^{-4}$, where the range comes from different event generators PYTHIA and MC@NLO+HERWIG. Additionally including the $p_T(ZZ)$ distribution in the probability calculation results in the range becoming $(2.7 - 10.5) \times 10^{-5}$. These probabilities depend on the chosen M_{ZZ} cutoff of $300\,\mathrm{GeV}/c^2$. If the $p_T(ZZ)$ distribution for the four high-mass events is considered on its own, the probability of its likelihood being less than that observed in the data is $(1.2 - 4.3) \times 10^{-4}$.

V. $ZZ \to \ell^+\ell^-\nu\nu$ CHANNEL

The four-lepton events observed above $300\,\mathrm{GeV}/c^2$ appear somewhat anomalous. If these events were due to a new ZZ resonance, it would also be detectable in the other ZZ decay modes, $\ell\ell + \not\!\!E_T$ and $\ell\ell jj$. Z bosons coming from the decay of such a heavy particle would be boosted, so events with one of the Z bosons decaying into neutrinos would have large $\not\!\!E_T$. For each lepton flavour, the branching ratio into neutrinos is twice that of charged leptons. With all three neutrino flavors included, and only one Z boson to be reconstructed, the expected event yield is around ten times higher than in the $\ell\ell\ell\ell$ channel, and the sensitivity to new physics at $M_{ZZ} = 325\,\mathrm{GeV}/c^2$ is several times better than in the $\ell\ell\ell\ell$ channel.

Optimising sensitivity for a resonance of mass $M_{ZZ} \sim 325\,\mathrm{GeV}/c^2$ we define the search region to be $\not\!\!E_T > 100\,\mathrm{GeV}$. The standard model expectation for events with a $Z \to \ell^+\ell^-$ candidate and such high $\not\!\!E_T$ is of the order of 25 events, as given in Table II. $Z \to e^+e^-$ and $Z \to \mu^+\mu^-$ candidates are selected according to the requirements described for the $ZZ \to \ell^+\ell^-\ell^+\ell^-$ channel. Owing to the extra acceptance, we do not reprocess the $\ell\ell + \not\!\!E_T$ data.

TABLE I: Four-lepton candidate events.

leptons	$M_{Z_1}, p_T(Z_1)$ (GeV/c^2), (GeV/c)	$M_{Z_2}, p_T(Z_2)$ (GeV/c^2), (GeV/c)	M_{ZZ} (GeV/c^2)	$p_T(ZZ)$ (GeV/c)	$\not\!\!E_T$ (GeV)	N_{jets}	Jet E_T (GeV)
$eeee$	93.3, 18.2	92.9, 17.4	196.6	35	14	0	
$\mu\mu\mu\mu$	85.9, 101.9	92.1, 54.8	321.1	47.4	8.4	1	36.7
$ee\mu\mu$	92.0, 156.0	89.9, 139.7	324.7	126.8	31	2	97.4, 40.0
$eeee$	101.3, 57.8	91.6, 13.2	334.4	44.7	9.9	1	22.7
$ee\mu\mu$	87.9, 17.7	91.8, 29.8	191.8	31	10.5	0	
$\mu\mu\mu\mu$	95.9, 197.9	92.0, 87.2	329.0	110.9	23.3	2	97.2, 24.7
$ee\mu\mu$	95.2, 36.7	89.7, 38.8	237.5	10.2	1.2	0	
$\mu\mu\mu\mu$	88.4, 51.0	89.8, 26.6	194.1	25.9	3.3	0	

We validate the background model using events with a reconstructed Z boson and $\not\!\!E_T < 100\,\text{GeV}$. Irreducible background contributions to a search for new physics in this channel come from standard model diboson production processes WW, WZ, and ZZ, as well as from top-quark production. Other non-negligible background contributions come from Z+jets events that have large $\not\!\!E_T$ due to jet mismeasurement; from W+jets events where one of the jets is misreconstructed as a lepton and forms a Z boson candidate with the charged lepton from the decay of the W boson; and, in the $ee + \not\!\!E_T$ channel, from $W\gamma$ production with the photon misreconstructed as an electron.

Irreducible backgrounds are estimated using the PYTHIA generator and the full CDF detector simulation, normalized to NLO cross sections [23]. The Z+jets contribution is also estimated using PYTHIA simulation and is normalised using a subset of the $\not\!\!E_T < 100\,\text{GeV}$ data. As Z+jets events have high $\not\!\!E_T$ only through misreconstruction, the normalisation is carried out on events having $50 < \not\!\!E_T < 100\,\text{GeV}$ that also have a small angle $\Delta\phi_{\text{min}}$ between the $\not\!\!E_T$ and the closest jet, or lepton, reconstructed in the event: $-0.5 < \Delta\phi_{\text{min}} < 0.5$. The distribution is shown in Fig. 7.a. It is verified that this procedure is not sensitive to the $\not\!\!E_T$ range used.

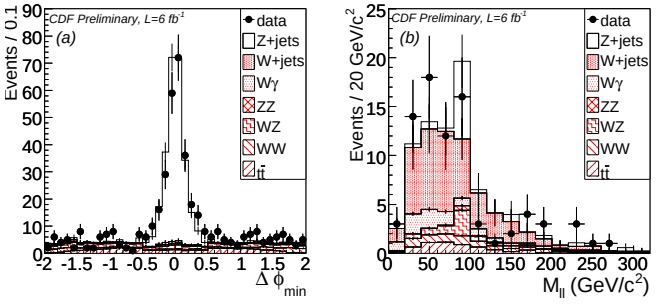

FIG. 7: (a) $\Delta\phi_{\text{min}}$ as used for Z+jets normalization, and (b) $M_{\ell\ell}$ for same-sign dielectron pairs with large $\not\!\!E_T$ used to validate the W+jets background estimation.

The background contribution from the W+jets process is estimated from a data sample where events contain an identified lepton and an additional jet. These events are weighted by jet-to-lepton misidentification rates as described in Section IV to estimate the total yield. Owing to differences in jet-to-lepton fake rates between electrons and muons, the W+jets contribution is found to be negligible in the $\mu\mu + \not\!\!E_T$ channel, but non-negligible in the $ee + \not\!\!E_T$ channel.

Photon conversions are the major source of jets being misidentified as electrons, and so W+jets events result in approximately equal numbers of same-charged and oppositely-charged candidate events. The estimate is therefore validated against the sample of events that have two lepton candidates of the same charge and $50 < \not\!\!E_T < 100\,\text{GeV}$. Fig. 7.b shows that this selection is dominated by W+jets. The estimate is also cross-checked by applying the same misidentification rates to $W^{\pm} \to e^{\pm}\nu$ simulation normalised to the NLO production cross section. This gives a consistent result within 10%.

The overall modeling of the sample composition is demonstrated by the $\not\!\!E_T$ spectrum shown in Fig. 8. The

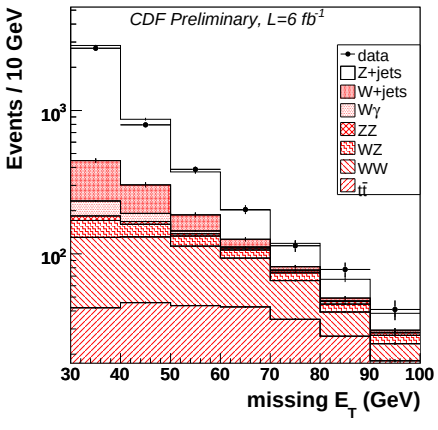

FIG. 8: $\not\!\!E_T$ distribution for events with opposite sign lepton pairs ($ee + \mu\mu$). The contribution of Z+jets events is normalized in the region $50\,\text{GeV} < \not\!\!E_T < 100\,\text{GeV}$ using events with low $|\Delta\phi_{\text{min}}|$.

.

The largest uncertainty in this channel is owing to the Z+jets

normalisation, and is 10% and 13% in the electron and muon channels respectively. Other uncertainties come from lepton identification (2%), acceptance (<1%), cross sections of diboson and top-quark production (5% and 10%), and the fake lepton background (20%). The total background uncertainty is 13%.

A. $ZZ \to \ell^+\ell^-\nu\nu$ high-mass search results

As the second Z boson in this channel decays into neutrinos, the invariant mass of the Z pair cannot be fully reconstructed. The closest approximation is the 'visible mass' $M_{ZZ}^{\rm vis}$, defined as the invariant mass of the sum of the two charged lepton four-momenta and the four-vector representing the $\not\!\!E_T$, $(\not\!\!E_x, \not\!\!E_y, 0, |\not\!\!E_T|)$. Fig. 9 shows the $M_{ZZ}^{\rm vis}$ distribution in the signal region $\not\!\!E_T > 100\,\text{GeV}$, with the expected distribution for an RS graviton of mass $M_{G*} = 325\,\text{GeV}/c^2$ overlaid. Four four-lepton events around $M_{ZZ} = 325\,\text{GeV}/c^2$ coming from the decay of a new state would imply a production cross section times branching ratio to ZZ close to 1 pb, so all the signal distributions displayed are normalised to that value. The three high-$M_{ZZ}^{\rm vis}$ events in the electron channel have high levels of jet activity.

Event yields are given in Table II, with expected signal yields for both s-channel and boosted G^* signal models. In this channel we find little difference in expected distributions or yields between the two signal models, confirming that the analysis is not strongly dependent on the detail of the model. In $ee + \not\!\!E_T$ and $\mu\mu + \not\!\!E_T$ channels combined we expect to observe 26 events from standard model processes and observe 27, giving no evidence for a resonance decaying into ZZ.

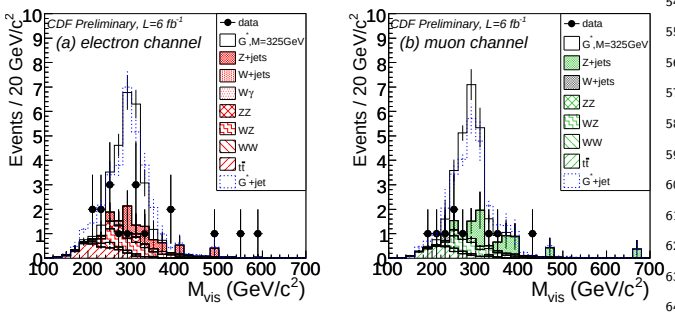

FIG. 9: $M_{ZZ}^{\rm vis}$ for (a) the electron and (b) muon channels. The expected contribution from a graviton of $M_{G^*} = 325\,\text{GeV}/c^2$ and cross section times branching ratio to ZZ of 1 pb is shown together with the expected contribution of boosted G^*, produced in association with a jet.

VI. $ZZ \to \ell^+\ell^- JJ$ CHANNEL

The decay of a heavy particle into two Z bosons where one of the Z bosons decays into charged leptons and the other to jets has the advantage of being fully reconstructible, and the event yield in the $\ell\ell jj$ channel is expected to be around twenty times higher than in the $\ell\ell\ell\ell$ channel.

TABLE II: Expected and observed event yields in the $\ell\ell + \not\!\!E_T$ channel.

Source	electron channel	muon channel
ZZ	1.8	1.3
WZ	3.6	2.8
WW	0.9	0.5
$t\bar{t}$	3.2	2.4
W+jets	0.1	0.3
Z+jets	4.0	5.1
Total standard model	13.6 ± 1.8	12.4 ± 1.6
Data	18	9
Expected s-channel signal, $M_G = 325\,\text{GeV}/c^2$ and σ=1 pb	17 ± 1	18 ± 1
Expected boosted signal, $M_G = 325\,\text{GeV}/c^2$ and σ=1 pb	20 ± 1	17 ± 1

$Z \to e^+e^-$ and $Z \to \mu^+\mu^-$ candidates are selected according to the requirements described for the $ZZ \to \ell^+\ell^-\ell^+\ell^-$ channel, and a further requirement is made of at least two reconstructed jets having E_T>25 GeV. To reconstruct the second Z boson candidate, all pairs of jets are considered and if there is a pair with invariant mass between 70 and $100\,\text{GeV}/c^2$ it is accepted. This inclusive selection, with the additional requirement of four-object invariant mass $M_{\ell\ell jj} < 300\,\text{GeV}/c^2$, defines a control region.

This channel is dominated by Z+jets events. Other standard model sources, small compared with Z+jets, are WZ and ZZ production, and top-quark production. The contributions from WW production and from W+jets events are negligible.

Diboson and top-quark event yields are estimated using PYTHIA Monte Carlo normalized to NLO cross sections. Z+jets events are modelled using the generator ALPGEN [24] interfaced with PYTHIA for parton showering, and the normalisation of the Z+jets contribution is obtained by fitting to the data in the control region. The detector acceptance is different for $Z \to e^+e^-$ and $Z \to \mu^+\mu^-$and so the Z+jets normalisation factors for the two channels are not expected to be identical. The difference between them is indicative of the systematic uncertainty, leading to a total background uncertainty of 10%. The distributions of number of jets in the control region, shown in Fig. 10, demonstrate the background modeling.

In the $\ell\ell jj$ final state we improve the resolution in the reconstructed M_{ZZ} by varying lepton and jet four-momenta within their uncertainties and constraining the reconstructed invariant masses $M_{\ell\ell}$ or M_{jj} to the mass of the Z boson, M_Z. In the $\ell\ell jj$ channel this improves the mass resolution of the ZZ candidates, and throughout this paper $M_{\ell\ell jj}$ refers to the constrained four-object invariant mass. It is verified that this procedure has little effect on events in the $\ell\ell\ell\ell$ final state, where it is used only as a cross-check.

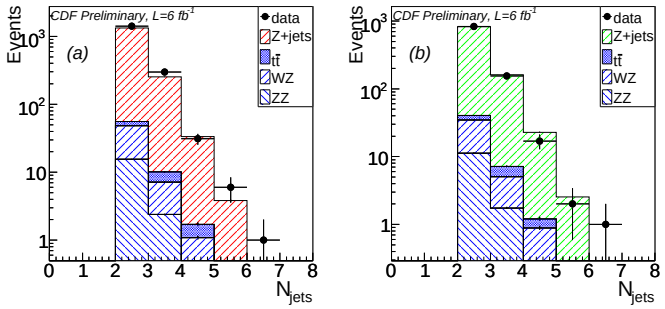

FIG. 10: Number of jets in (a) $Z \to e^+e^- + \geq 2$ jets and (b) $Z \to \mu^+\mu^- \geq 2$ jets events in the control region $M_{\ell\ell jj} < 300\,\mathrm{GeV}/c^2$.

A. $ZZ \to \ell^+\ell^- jj$ high-mass search results

As the $ZZ \to \ell^+\ell^- jj$ final state is fully reconstructed, a new resonance would manifest itself as a peak in $M_{\ell\ell jj}$. Z bosons coming from the decay of a heavy particle would be boosted, and optimisation studies result in requiring the leading jet in the $Z \to jj$ candidate to have $p_T > 50\,\mathrm{GeV}/c$ and the p_T of either the $Z \to jj$ or $Z \to \ell^+\ell^-$ candidate to be greater than $75\,\mathrm{GeV}/c$. Studies of systematic effects resulting from the generator Q^2 and from the jet energy scale uncertainty show that they do not affect the expected shapes of the $M_{\ell\ell jj}$ distributions.

Fig. 11 shows the $M_{\ell\ell jj}$ distribution for the $eejj$ and $\mu\mu jj$ channels with the prediction for a G^* of mass $M_{G^*} = 325\,\mathrm{GeV}/c^2$ and production cross section times branching fraction to ZZ of 1 pb. Observed event yields are given in Table III and are consistent with standard model expectation.

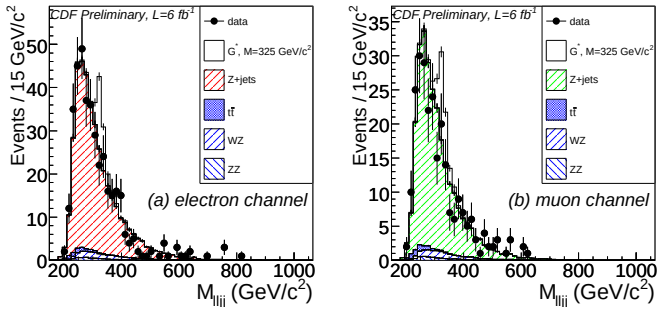

FIG. 11: $M_{\ell\ell jj}$ for the (a) electron and (b) muon channels, showing the expected contribution from a G^* of $M_{G^*} = 325\,\mathrm{GeV}/c^2$ and cross section times branching ratio to ZZ of 1 pb.

We investigate potential effects of the production mechanism using the alternative boosted G^* signal model. Motivated by the anomalous $p_T(ZZ)$ distribution shown by the events in the four lepton channel, the signal selection is modified to require $p_T(\ell\ell jj) > 40\,\mathrm{GeV}/c$, which further suppresses standard model background, and the resulting $M_{\ell\ell jj}$ distribution and boosted G^* prediction is shown in Fig. 12. As with the $\ell\ell + \not\!\!E_T$ channel there are no statistically significant fluctuations from the expectation.

TABLE III: Expected and observed event yields in the $\ell\ell jj$ channel.

Source	electron channel	muon channel
ZZ	6	5
WZ	17	12
$t\bar{t}$	7	5
Drell-Yan	395	244
Total standard model	424±40	266±24
Data	392	253
Expected signal, $M_G = 325\,\mathrm{GeV}/c^2$ and σ=1 pb	41±1	32±1

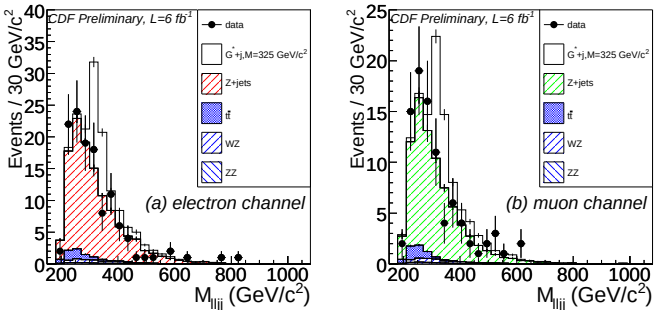

FIG. 12: $M_{\ell\ell jj}$ for the (a) electron and (b) muon channels for $p_T(ZZ) > 40\,\mathrm{GeV}/c$, showing the expected contribution from a boosted G^* of $M_{G^*} = 325\,\mathrm{GeV}/c^2$ and cross section times branching ratio to ZZ of 1 pb.

VII. LIMITS

To quantify results of the search we compute expected and observed limits on the production cross section times branching ratio $\sigma(p\bar{p} \to X \to ZZ)$.

The expected sensitivity is determined with a Bayesian technique [25], performing a binned maximum-likelihood fit over the M_{ZZ} and $M_{\ell\ell jj}$ distributions in the $\ell\ell\ell\ell$ and $\ell\ell jj$ channels respectively, and over the M_{ZZ}^{vis} distribution in the $\ell\ell + \not\!\!E_T$ channel. Background-only pseudo-experiments are drawn from Monte Carlo simulation. A test statistic is formed from the difference in the likelihoods between the background-only model and the signal-plus-background model at the best fit values for the pseudoexperiment. The background templates can fluctuate within their uncertainties, keeping their ratios constrained to those predicted by the standard model. From this, expected 95% credibility level (CL) upper limits on cross section times branching ratio are extracted.

Fig. 13 shows expected and observed limits in the

four-lepton channel for G^* masses between 250 and 1000 GeV/c^2. At $M_{G^*} = 325\,\mathrm{GeV}/c^2$ the expected sensitivity is around 0.7 pb, and the four events with masses clustered around that value result in an observed limit of 1.9 pb.

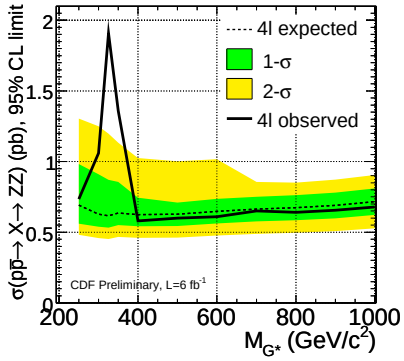

FIG. 13: Expected and observed 95% CL limits on $\sigma(p\bar{p} \to X \to ZZ)$ from the $ZZ \to \ell^+\ell^-\ell^+\ell^-$ channel; the four events with M_{ZZ}=327 GeV/c^2 result in a deviation from the expected limit.

Although the backgrounds in the $ee+\not\!\!E_T$ and $\mu\mu+\not\!\!E_T$ channels are higher than in the four lepton channel, those channels provide better sensitivity. Fig. 14.a shows the expected and observed cross section limits for $ee+\not\!\!E_T$ and $\mu\mu+\not\!\!E_T$ combined, and there are no large fluctuations from expectation. For $M_{G^*} = 325\,\mathrm{GeV}/c^2$ the expected 95% CL upper cross section limit is 0.29 pb and the observed limit is 0.25 pb. For the boosted G^* signal model the 95% CL expected and observed limits are both 0.30 pb. This is a change of less than 10% from the s-channel model, demonstrating that the analysis sensitivity is not strongly dependent on the detail of the production model.

Fig. 14.b shows the expected and observed cross section limits for the $\ell\ell jj$ channel. Here the expected 95% CL upper cross section limit is 0.38 pb for $M_{G^*} = 325\,\mathrm{GeV}/c^2$, and the observed limit is 0.23 pb. With the selection modified for a boosted signal model, $p_T(\ell\ell jj) > 40\,\mathrm{GeV}/c$, the sensitivity is improved slightly compared to the s-channel signal model. The expected limit is 0.27 pb and the observed limit is 0.26 pb, showing that also in this channel the analysis sensitivity is not strongly dependent on the detail of the signal model.

Combining all three channels results in expected and observed limits that are consistent with each other, shown in Fig. 15. For $M_{G^*} = 325\,\mathrm{GeV}/c^2$ the sensitivity is dominated by the $\ell\ell + \not\!\!E_T$ channel. For an s-channel resonance, the 95% CL upper cross section limit is expected to be 0.19 pb and is observed to be 0.26 pb. For a boosted resonance of $M_{G^*} = 325\,\mathrm{GeV}/c^2$ the expected limit is 0.17 pb and the observed limit is 0.28 pb. The difference between the expected and observed limits is due to the events observed in the four-lepton channel.

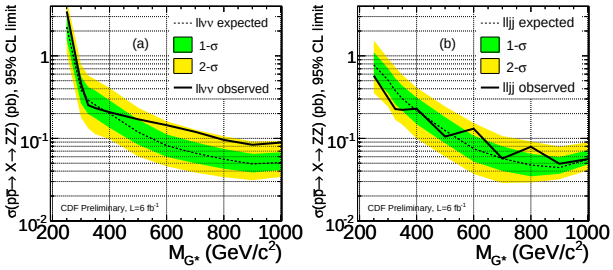

FIG. 14: Expected and observed 95% CL limits on $\sigma(p\bar{p} \to X \to ZZ)$ from (a) the $ZZ \to \ell^+\ell^-\nu\nu$ channel, and (b) the $ZZ \to \ell^+\ell^- jj$ channel.

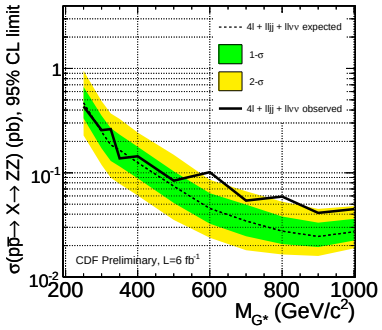

FIG. 15: Expected and observed 95% CL limits on $\sigma(p\bar{p} \to X \to ZZ)$ from all channels combined.

VIII. CONCLUSIONS

In conclusion, we have searched for heavy resonances decaying into Z boson pairs using the final states consisting of four charged leptons, two leptons and $\not\!\!E_T$, and two leptons plus jets. In the $ZZ \to \ell^+\ell^-\ell^+\ell^-$ channel we have observed eight candidate events. The M_{ZZ} and $p_T(ZZ)$ distributions of these events are different from those expected from the standard model. Four high-mass $ZZ \to \ell^+\ell^-\ell^+\ell^-$ candidates have M_{ZZ} consistent with 327 GeV/c^2 within detector resolution, and high values of $p_T(ZZ)$. The probability to observe such distributions from standard model sources is $(2.7 - 10.5) \times 10^{-5}$, where the range comes from different event generators.

However, searches in the $\ell\ell + \not\!\!E_T$ and $\ell\ell jj$ final states do not confirm a signal of a new heavy particle decaying to two Z bosons. We set upper limits on the cross section times branching ratio $\sigma(p\bar{p} \to X \to ZZ)$: at $M = 325\,\mathrm{GeV}/c^2$ these limits are 0.26 pb and 0.28 pb, at 95% CL, for two RS graviton signal models.

We thank the Fermilab staff and the technical staffs of the participating institutions for their vital contributions.

This work was supported by the U.S. Department of Energy and National Science Foundation; the Italian Istituto Nazionale di Fisica Nucleare; the Ministry of Education, Culture, Sports, Science and Technology of Japan;

the Natural Sciences and Engineering Research Council of Canada; the National Science Council of the Republic of China; the Swiss National Science Foundation; the A.P. Sloan Foundation; the Bundesministerium für Bildung und Forschung, Germany; the Korean Science and Engineering Foundation and the Korean Research Foundation; the Science and Technology Facilities Council and the Royal Society, UK; the Institut National de Physique Nucleaire et Physique des Particules/CNRS; the Russian Foundation for Basic Research; the Comisión Interministerial de Ciencia y Tecnología, Spain; the European Community's Human Potential Programme under contract HPRN-CT-2002-00292; and the Academy of Finland.

[1] M. Kober, B. Koch and M. Bleicher, Phys. Rev. D **76** 125001 (2007).

[2] L. Randall and R. Sundrum, Phys. Rev. D **83** 4690 (1999).

[3] D. de Florian and M. Grazzini, Phys. Lett. B **674** (2009) 291.
C. Anastasiou, R. Boughezal, and F. Petriello, J. High Energy Phys. **0904** (2009) 003.
A. Djouadi, J. Kalinowski and M. Spira, Comp. Phys. Commun. **108 C** (1998) 56.

[4] The coupling must be large enough to be consistent with the apparent weakness of gravity but small enough to prevent the theory from becoming nonperturbative and a natural choice is $k/M_{Pl} = 0.1$, where k is a curvature parameter and M_{Pl} is the Planck scale.

[5] T. Aaltonen *et al.* (CDF-II Collaboration), FERMILAB-PUB-11-178-E (arXiv:1103.4650, submitted to Phys. Rev. Lett.).
V. Abazov *et al.* (D0 Collaboration), Phys. Lett. B **695** 88 (2011).
G. Aad *et al.* (ATLAS Collaboration) Phys. Lett. B (in press) doi:10.1016/j.physletb.2011.04.044.
S. Chatrchyan *et al.* (CMS Collaboration) CERN-PH-EP-2011-002, CERN-PH-EP-2011-020.

[6] K. Agashe, H. Davoudiasl, G. Perez, A. Soni, Phys. Rev. D **76** 036006 (2007).

[7] L. Fitzpatrick, J. Kaplan, L. Randall and L. Wang, J. High Energy Phys. **0709** (2007) 013.

[8] T. Aaltonen *et al.* (CDF-II Collaboration), FERMILAB-PUB-11-036-E (arXiv:1102.4566, submitted to Phys. Rev. D)

[9] R. Blair *et al.* (CDF-II Collaboration), FERMILAB-Pub-96/390-E.

[10] A. Sill *et al.*, Nucl. Instrum. Methods Phys. Res. A **447** 1 (2000).

[11] T. Affolder *et al.*, Nucl. Instrum. Methods Phys. Res. A **526**, 249 (2004).

[12] L. Balka *et al.*, Nucl. Instrum. Methods Phys. Res. A **267** 272 (1988).

[13] S. Bertolucci *et al.*, Nucl. Instrum. Methods Phys. Res. A **267** 301 (1988).

[14] G. Ascoli *et al.*, Nucl. Instrum. Methods Phys. Res. A**268** 33 (1988).

[15] D. Acosta *et al.*, Nucl. Instrum. Methods Phys. Res. A **494** 57 (2002).

[16] A. Abulencia *et al.* (CDF collaboration), J. Phys. G Nucl. Part. Phys. **34** 2457 (2007).

[17] F. Abe *et al.* (CDF collaboration), Phys. Rev. D **45** 1448 (1992).

[18] T. Sjöstrand *et al.*, Comput. Phys. Commun. **135**, 238 (2001).

[19] E. Gerchtein and M. Paulini, CHEP-2003-TUMT005.

[20] S. Frixione and B. R. Webber, J. High Energy Phys. **0206** (2002) 029.

[21] G. Corcella *et al.*, J. High Energy Phys. **01** (2001) 010.

[22] G. J. Feldman and R. D. Cousins, Phys. Rev. D **57** 3873 (1998).

[23] J. M. Campbell and R. K. Ellis, Phys. Rev. D **60** 113006 (1999).
N. Kidonakis, R. Vogt, Phys. Rev. D **78** 074005 (2008).

[24] M. L. Mangano *et al.*, J. High Energy Phys. **0307** (2003) 001.

[25] J. Heinrich and L. Lyons, Annual Review of Nuclear and Particle Science **57** 145 (2007).